ChemPubSoc Europe

DOI: 10.1002/celc.201402328

CHEMELECTROCHEM Communications

Delivery of Single Nanoparticles from Nanopipettes under Resistive-Pulse Control

Yixian Wang, Huijing Cai, and Michael V. Mirkin*[a]

In this communication we show that the resistive-pulse setup can be employed to control the delivery of single nanoparticles from a nanopipette. The precise pipette positioning for local delivery of nanoparticles can be attained by using it as a scanning ion-conductance microscopy (SICM) tip. Experimental SICM approach curves fit the developed theory well.

Electrochemistry of nanometer-sized electroactive species such as vesicles, nanoparticles (NPs), and large biomolecules is of significant current interest.[1,2] Metal NPs are particularly important because of their applications in catalysis, sensors, and healthcare.[3–5] Most published electrochemical experiments involved a large number of NPs and particle ensembles. Experiments at the single-NP level could help elucidate the relationships between the NP shape, size and orientation on the surface and its electrochemical or catalytic properties[3] and improve understanding of NP interactions with biomembranes[6a] and cytotoxicity.[6b] Different approaches to local delivery of NPs[7] and biomolecules[8,9] have recently been reported, however, controlled delivery of single nanoscale species has yet to be attained.

This communication is aimed at developing new nanoelectrochemical methodology for controlled delivery of single-nanometer-sized particles. The delivery system is based on the resistive-pulse concept,[10] which has been widely employed in sensing applications from single-molecule detection[11] to particle sizing[12] to DNA sequencing.[13] In a conventional resistive-pulse experiment, the ion current (i_0) flows through a small pore (Figure 1A) driven by the voltage (V) applied between two reference electrodes positioned on the opposite sides of the orifice. A single particle can enter the pore and partially block the current (Figure 1B). The resulting spike in the current versus time curve (resistive pulse) is used to detect the particle. A detectable particle must be sufficiently small to pass through the orifice, but at the same time large enough to cause measurable change in the recorded ion current, Δi. Individual blockage events on the millisecond or sub-millisecond time scale can be recorded using a patch clamp amplifier or a similar device.

Most reported resistive-pulse experiments were performed with biological or solid-state nanopores, and only a few studies employed nanopipettes.[12b,14,15] We recently showed the possibility of using nanopipettes for resistive-pulse sensing of Au nanoparticles (AuNP), nanoparticles coated with an allergen epitope peptide layer, AuNP with bound antipeanut antibodies[16a] and protein biomarker.[16b] Similarly to a nanopore, a nanopipette can sense the analyte species entering and partially blocking its nanometer-sized orifice.[8a] A nanopipette offers several important advantages, including the ease of fabrication, small physical size (the outer diameter of the pipette tip can be as small as $\leq$10 nm),[17] and the needle-like geometry, which makes it suitable as a tip for scanning probe microscopies.[8] One can use the scanning electrochemical microscope (SECM)[18] or scanning ion-conductance microscope (SICM)[19] to precisely position a nanopipette near the substrate in order to deliver nanoparticles to its surface. A pipette with a radius as small as ~8 nm has previously been used in an SECM experiment, and the minimum attainable separation distance was $<$1 nm.[20] Similar positioning capabilities can be expected for SICM.

The concept of the particle delivery under resistive-pulse control is illustrated in Figure 1C. In this case, nanoparticles are initially present in the filling solution inside the nanopipette, and suitable voltage is applied between two reference electrodes to drive the particles from the pipette to the external solution (note the reversed voltage polarity and current direction in Figure 1C). A current spike should occur every time when a particle is ejected from the pipette, thus enabling precise control of the number of particles delivered. In resistive-pulse experiments with pressure-induced flow, Lan and White[21] showed that relatively large (120–160 nm) NPs can be ejected from a conical nanopore ("release translocation") by reversing the applied pressure. Although the inside geometry of conical nanopores is similar to that of nanopipettes, a nanopore is not a suitable tool for localized delivery because of the large outer diameter of its glass wall.

Two different kinds of NPs were used in our experiments: commercial gold nanoparticles (AuNPs; either 10 or 20 nm diameter) and much larger AuNP-antibody-antigen particles prepared in James Rusling's laboratory at the University of Connecticut[16b] (Supporting Information). Figure 2 shows three current–time recordings obtained with an 18 nm-diameter borosilicate pipette. No current blockages can be seen in the background trace obtained with no particles added to either external or inner solution (Figure 2A). When negatively charged citrate-stabilized 10 nm AuNPs were added to the ex-

[a] Dr. Y. Wang,[+] H. Cai, Prof. M. V. Mirkin
Department of Chemistry and Biochemistry
Queens College-CUNY
Flushing, New York 11367 (USA)
E-mail: mmirkin@qc.cuny.edu

[+] Current Address:
Center for Bioelectronics and Biosensors
Biodesign Institute, Arizona State University
Tempe, AZ 85287-6206 (USA)

Supporting Information for this article is available on the WWW under http://dx.doi.org/10.1002/celc.201402328.

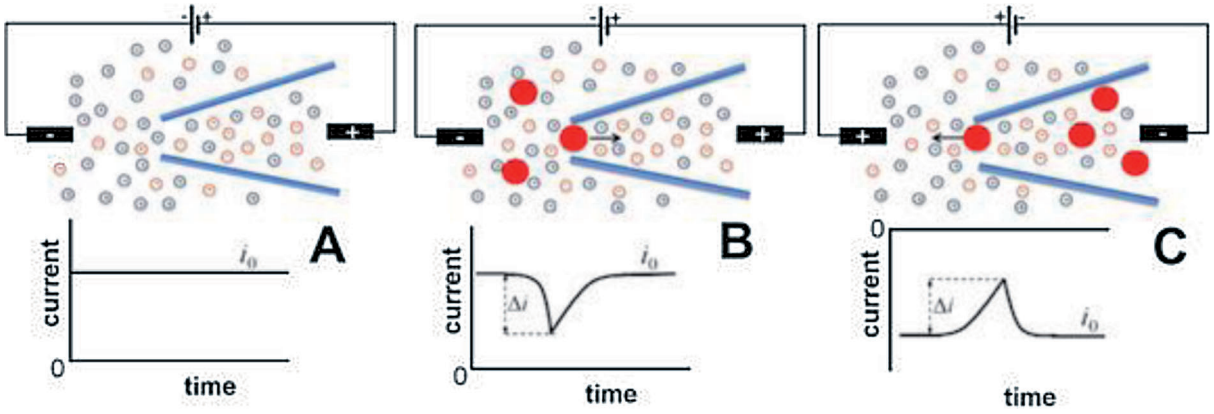

Figure 1. Simplified schematic representation of resistive-pulse sensing and particle delivery with a nanopipette. A) With no particles present in solution, essentially constant ion current (i_0) flows through the orifice. B) In the presence of nanoparticles in external solution, individual blockage events can be seen in the current versus time curve. C) A resistive pulse is produced by the particle ejection from the pipette to the external solution.

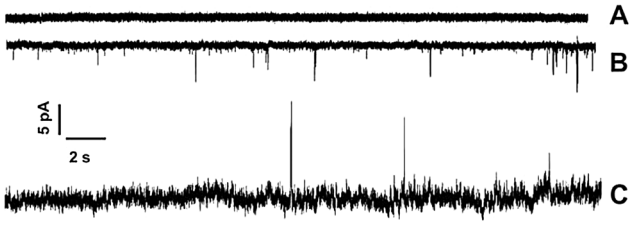

Figure 2. Current–time recordings obtained with an 18 nm-diameter pipette in the 15 mM NaCl + 13 mM phosphate buffer (pH7) and A) no AuNP in solution, B) 1.9 nM of 10 nm-diameter AuNP in the external solution, and C) 1.9 nM AuNP in the filling solution. A) $V = 200$ mV, $i_0 = 38$ pA; B) $V = 200$ mV, $i_0 = 23$ pA; C) $V = -120$ mV, $i_0 = -62$ pA. The upward spikes in (C) correspond to the decrease in the magnitude of negative current. Sampling frequency was 100 kHz, and the low-pass-filter bandwidth was 10 kHz. The pipettes in (B) and (C) are two halves pulled from the same capillary.

ternal solution, their translocation through a nanopipette produced a number of pulses with the current changes much larger than the noise level (Figure 2B). When the same NPs were added to the filling solution, current blockages corresponding to the expulsion of negatively charged particles from the pipette appeared at negative potentials applied to the inner reference electrode (Figure 2C).

A significantly lower frequency of current blockages for the ejection of the NPs from the pipette (Figure 2C) than for the opposite process (Figure 2B) reflects slower transport of NPs inside the pipette, where the direction of the electroosmotic flow was opposite to that of the electrophoresis. For the controlled delivery of single NPs from the pipette, the optimal translocation frequency would be even lower (e.g., ~1–2 events per minute) to allow enough time for the pipette to be moved and avoid dispensing multiple particles at the same location. Several experimental parameters are expected to influence the frequency of NP translocations, including the applied voltage, surface charge density on the inner pipette wall, size and electrophoretic mobility of NPs, and geometry of the pipette inside. The current–time recording in Figure 3A obtained with a larger negative voltage ($V = -600$ mV) and higher electrolyte concentration exhibits a significantly higher frequency of resistive pulses. As in most reported resistive-pulse experiments, the pulse width and amplitude in Figure 3A varied significantly, but the shape of a typical pulse for the NP delivery (Figure 3B) is markedly different from that of a pulse produced by the NP entry into the pipette shaft (Figure 3C). In the latter case, the characteristic asymmetrical spikes exhibit the sharp initial decrease in current followed by a slow relaxation (tail), as discussed earlier for both nanopores[11a,21,22] and pipettes.[16a] This shape reflects the changes in the pipette's resistance, which increases sharply

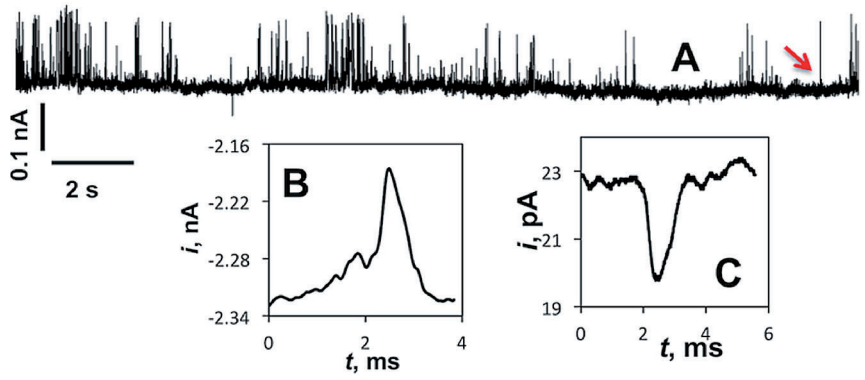

Figure 3. A) Current–time recordings obtained with a 40 nm-diameter pipette in the 60 mM NaCl + 60 mM phosphate buffer (pH 7) and 1.9 nM of 20 nm-diameter AuNP in filling solution. $V = -600$ mV, $i_0 = -2.32$ nA. The trace was originally recorded at 14 kHz filter bandwidth and postfiltered at 3 kHz. The upward spikes correspond to the decrease in the magnitude of negative current. B) Close-up of the pulse marked with a red arrow in (A). C) Close-up of a pulse from Figure 2B.

when the particle enters the pipette and then decreases slowly. For the NP delivery, the reversal of the pulse shape can be expected because the solution resistance in the tapered narrow shaft of the pipette should increase slowly as the NP approaches the orifice and then abruptly decrease when the particle is released (Figure 3B). Similar shape reversal has been observed in current pulses corresponding to the pressure-driven capture and release of NPs using conical nanopores.[23]

The delivery of more complex NPs from larger nanopipettes to the external solution is shown in Figure 4. These negatively charged particles, AuNP-mAb-VEGF-C, were prepared by conjugating AuNPs with monoclonal antibodies (mAb) and subsequent attachment of VEGF-C antigen.[16c] Unlike the AuNPs in Figures 2 and 3, AuNP-mAb-VEGF-C are polydisperse with the radius values ranging from ~40 to ~60 nm.[16b] Additionally, the filling solution could contain some smaller AuNP-mAb particles without attached protein. Resistive-pulse recordings corresponding to the delivery of these particles from the 168 nm-radius pipette (Figure 4A) contain different types of pulses, most of which show increases in the absolute value of the ion current. The increase in current during the translocation event was observed previously and attributed to the charge on the particle itself[24a] and the motion of the counterions.[24b] The pulses produced by AuNP-peptide-antipeanut antibody translocation also showed increases in the current magnitude.[16a] The aforementioned reversal of the pulse shape (see Figure 3B and related discussion), that is, the slow increase in current as the NP approaches the orifice and subsequent abrupt decrease when the particle is released, can be seen in Figure 4B.

Another type of current pulses are shown in Figure 4A, namely biphasic pulses in which a current increase is followed by a decrease (Figure 4C). Somewhat similar biphasic pulses were recorded experimentally and simulated for the pressure-driven translocation of negatively charged NPs though glass nanopores with negative voltage values applied across the pore.[25] According to Ref. [25], the appearance of biphasic current pulses is due to the opposing effects of ion accumulation and volume exclusion produced by the NP translocation. One should also notice that the zeta potential of AuNP-mAb-VEGF-C (−14.0 ± 0.5 mV) was much less negative than that of bare gold nanoparticles (−45 ± 2.2 mV).[16b]

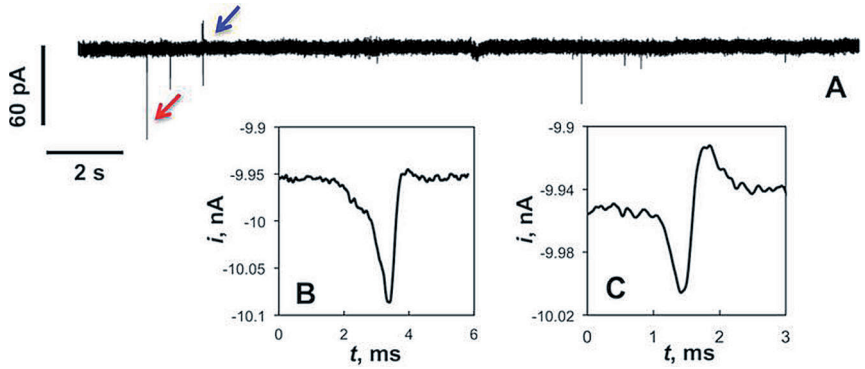

Figure 4. Current–time recordings obtained with a 168 nm-radius pipette in the 15 mM NaCl + 10 mM phosphate buffer (pH7) and 0.9 nM AuNP-mAb-VEGF-C in the internal solution. $V = -600$ mV, $i_0 = -9.96$ nA. The downward spikes correspond to the increase in the magnitude of the negative current. The current pulses marked with a red (B) and blue (C) arrows in (A). The trace was recorded at 10 kHz filter bandwidth and postfiltered at 5 kHz.

To deliver NPs locally, one has to bring a nanopipette close (e.g., to within 1–2 pipette radii) to the sample surface and precisely position it at the right distance above the desired spot. SICM can be used as a positioning technique compatible with the resistive-pulse-controlled delivery discussed above. A simple approach to controlling the distance between the nanopipette serving as an SICM tip and the substrate is the nonmodulated dc feedback mode with a constant potential value applied between the internal and external reference electrodes.[19c] The current versus distance curve can be obtained with the applied voltage at which NPs are not ejected from the pipette. (After the pipette is positioned, V can be switched to a value suitable for NP delivery.) By fitting the current–distance curve to the theory, one can establish the distance scale and precisely position the SICM tip in close proximity to the substrate.[26] The current is controlled by the ohmic resistance between the reference electrodes inside the pipette and in the external solution. When the pipette approaches the substrate impermeable to ions, the ion current decreases because of increasing resistance.[19]

The shape of the current–distance curve depends on the pipette geometry, including its radius (a), tapper angle (θ) and $RG = r_g/a$ (r_g is the outer pipette radius at the tip).[26] Our simulated current–distance curves (see the Supporting Information for problem formulation and COMSOL simulations) are in agreement with simulations reported in Ref. [26]. The theoretical approximation proposed in that article (Eq. (7) in Ref. [26]) was derived for RG = 10, which is much larger than a typical value for a quartz or glass nanopipette. By making use of the previously reported approximation for the negative-feedback SECM approach curve[27] and taking into account the internal pipette resistance, we obtained Equation (1), which is valid for a wide range of RG values:

$$\frac{i}{i_0} = \frac{\frac{\pi}{4} + \frac{1}{\tan\theta}}{\frac{\pi}{4}\frac{\frac{2.08}{RG^{0.358}}(L + 0.0023RG) + 1.57 + \frac{\ln RG}{L} + \frac{2}{\pi RG}\ln\left(1 + \frac{\pi RG}{2L}\right)}{\frac{2.08}{RG^{0.358}}\left(L - \frac{0.145}{RG}\right) + 1.585}} + \frac{1}{\tan\theta} \quad (1)$$

where L is the distance between the pipette orifice and the substrate normalized by a, and i/i_0 is the ion current normalized by the current value at infinite L.

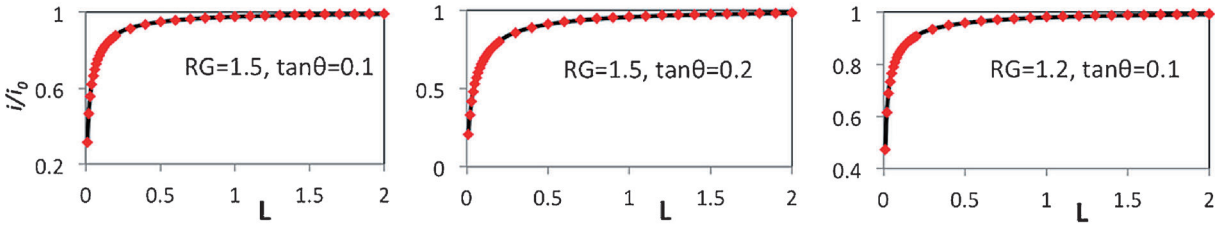

Figure 5. Dimensionless SICM approach curves for different combinations of parameters defining the pipette geometry. Symbols represent simulated data and solid curves are calculated from Equation (1).

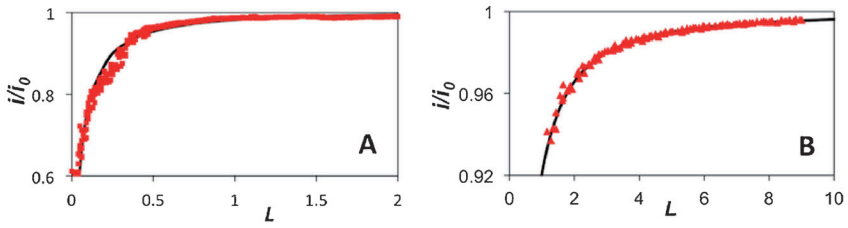

Figure 6. Experimental (symbols) and theoretical (solid) SICM approach curves obtained with a A) 100 nm-radius pipette and B) 32 nm-radius pipette. Both filling and external solutions contained 15 mM NaCl + 10 mM phosphate buffer (pH 7). Theoretical curves were calculated from Equation (1).

Figure 5 shows current–distance curves calculated from Equation (1) for different combinations of RG and θ (solid lines) and corresponding simulated curves (symbols). For $0.01 \leq L \leq 3$, $0.01 \leq \mathrm{RG} \leq 3$ and $5^\circ \leq \theta \leq 15^\circ$, the current values calculated from Equation (1) agree with results of COMSOL simulations within $<1\%$, which is smaller than the experimental uncertainty.

Figure 6 shows two experimental approach curves (symbols) obtained with a 100 nm (A) and 32 nm radius (B) pipettes. Both curves fit the theory very well and the separation distance at the point of the closest approach in either case is <50 nm, indicating that SICM can be used to precisely position a pipette near the substrate surface for subsequent NP delivery.

Importantly, SICM-based positioning (and re-positioning) can be performed with the pipette biased at a voltage at which no NPs are expelled to the external solution and then switching the voltage to a different value to effect the NP delivery. The careful control of the pipette bias should allow one to avoid complications, such the increase in ion current at closer distances between the nanopipette and an insulating surface due to electroosmotic flow separation reported recently by the Klenerman group.[28]

In summary, we developed the framework for single-particle delivery from nanopipettes. The two key aspects of these experiments are the resistive-pulse control that enables the delivery of the exact number of particles and the ability to bring a nanopipette within close proximity of the sample and position it with nm-scale precision. By using a pipette with a suitable aperture radius, one can obtain a current pulse much larger than the noise level for the ejection of each particle, as shown here for citrate-stabilized 10 nm AuNPs and much larger particles conjugated to antibodies and a protein biomarker. Similarly to previously reported resistive-pulse sensing experiments,[16a] the radius of a pipette suitable for the NP delivery was ~1.5–3 times that of the translocating particle.

The pipette positioning was achieved by using it as an SICM tip. An analytical approximation was developed to calculate the approach curve that fitted well experimental current-distance curves for different size pipettes. Experiments aimed at surface patterning with NPs delivered from nanopipettes under resistive-pulse control are underway in our laboratory.

Acknowledgement

This work was supported by the National Science Foundation (CHE-1300158) and the Air Force Office of Scientific Research Multi-University Research Initiative (FA9550-14-1-0003). We thank Prof. James Rusling and Snehasis Bhakta (University of Connecticut) for providing nanoparticles used in some resistive-pulse experiments and Yun Yu for his assistance with TEM imaging. The Supporting Information contains the experimental details, mathematical model and COMSOL simulation report.

Keywords: nanoelectrochemistry · nanoparticles · nanopipettes · resistive-pulse setups · scanning ion-conductance microscopy

[1] R. W. Murray, *Chem. Rev.* **2008**, *108*, 2688–2720.
[2] F. Scholz, *J. Solid State Electrochem.* **2011**, *15*, 1699–1702.
[3] S. E. F. Kleijn, S. C. S. Lai, M. T. M. Koper, P. R. Unwin, *Angew. Chem. Int. Ed.* **2014**, *53*, 3558–3586.
[4] D. L. Feldheim, C. A. Foss, *Metal Nanoparticles: Synthesis, Characterization, and Applications*, Marcel Dekker, New York, **2002**.
[5] F. P. Zamborini, L. Bao, R. Dasari, *Anal. Chem.* **2012**, *84*, 541–576.
[6] a) P. R. Leroueil, S. Hong, A. Mecke, J. R. Baker, B. G. Orr, M. M. Banaszak Holl, *Acc. Chem. Res.* **2007**, *40*, 335–342; b) H. Hess, Y. Tseng, *ACS Nano* **2007**, *1*, 390–392.
[7] S. E. F. Kleijn, S. C. S. Lai, T. S. Miller, A. I. Yanson, M. T. M. Koper, P. R. Unwin, *J. Am. Chem. Soc.* **2012**, *134*, 18558–18561.

[8] a) C. Morris, A. K. Friedman, L. A. Baker, *Analyst* **2010**, *135*, 2190 – 2202; b) W. Shi, N. Sa, R. Thakara, L. A. Baker, *Analyst*, **2015**, DOI: 10.1039/C4AN01073F.

[9] a) Y. Takahashi, A. I. Shevchuk, P. Novak, Y. Zhang, N. Ebejer, J. V. Macpherson, P. R. Unwin, A J. Pollard, D. Roy, C. A. Clifford, H. Shiku, T. Matsue, D. Klenerman, Y. E. Korchev, *Angew. Chem. Int. Ed.* **2011**, *50*, 9638 – 9642; *Angew. Chem.* **2011**, *123*, 9812 – 9816; b) B. Babakinejad, P. Jönsson, A. L. Córdoba, P. Actis, P. Novak, Y. Takahashi, A. Shevchuk, U. Anand, P. Anand, A. Drews, A. Ferrer-Montiel, D. Klenerman, Y. E. Korchev, *Anal. Chem.* **2013**, *85*, 9333 – 9342.

[10] a) H. Bayley, C. R. Martin, *Chem. Rev.* **2000**, *100*, 2575 – 2594; b) L. Luo, S. R. German, W.-J. Lan, D. A. Holden, T. L. Mega, H. S. White, *Annu. Rev. Anal. Chem.* **2014**, *7*, 513 – 535; c) I. Makra, R. E. Gyurcsányi, *Electrochem. Commun.* **2014**, *43*, 55 – 59.

[11] a) E. A. Heins, Z. S. Siwy, L. A. Baker, C. R. Martin, *Nano Lett.* **2005**, *5*, 1824 – 1829; b) S. Howorka, Z. Siwy, *Chem. Soc. Rev.* **2009**, *38*, 2360 – 2384.

[12] a) R. Vogel, G. Willmott, D. Kozak, G. S. Roberts, W. Anderson, L. Groenewegen, B. Glossop, A. Barnett, A. Turner, M. Trau, *Anal. Chem.* **2011**, *83*, 3499 – 3506; b) P. Terejánszky, I. Makra, P. Fürjes, R. E. Gyurcsányi, *Anal. Chem.* **2014**, *86*, 4688 – 4697.

[13] D. Branton, D. W. Deamer, A. Marziali, H. Bayley, S. A. Benner, T. Butler, M. Di Ventra, S. Garaj, A. Hibbs, X. Huang, S. B. Jovanovich, P. S. Krstic, S. Lindsay, X. S. Ling, C. H. Mastrangelo, A. Meller, J. S. Oliver, Y. V. Pershin, J. M. Ramsey, R. Riehn, G. V. Soni, V. Tabard-Cossa, M. Wanunu, M. Wiggin, J. A. Schloss, *Nat. Biotechnol.* **2008**, *26*, 1146 – 1153.

[14] a) M. Karhanek, J. T. Kemp, N. Pourmand, R. W. Davis, C. D. Webb, *Nano Lett.* **2005**, *5*, 403 – 407; b) S. Umeharaa, M. Karhanek, R. W. Davis, N. Pourmand, *Proc. Natl. Acad. Sci. USA* **2009**, *106*, 4611 – 4616.

[15] C. Gao, S. Ding, Q. Tan, L.-Q. Gu, *Anal. Chem.* **2009**, *81*, 80 – 86.

[16] a) Y. Wang, K. Kececi, M. V. Mirkin, V. Mani, N. Sardesai, J. F. Rusling, *Chem. Sci.* **2013**, *4*, 655 – 663; b) H. Cai, Y. Wang, M. V. Mirkin, S. Bakta, G. Bishop, A. Joshi, J. F. Rusling, *unpublished results*; c) S. Krishnan, V. Mani, D. Wasalathanthri, C. V. Kumar, J. F. Rusling, *Angew. Chem. Int. Ed.* **2011**, *50*, 1175 – 1178; *Angew. Chem.* **2011**, *123*, 1207 – 1210.

[17] a) Y. Shao, M. V. Mirkin, *J. Am. Chem. Soc.* **1997**, *119*, 8103 – 8104; b) Q. Li, S. Xie, Z. Liang, X. Meng, S. Liu, H. H. Girault, Y. Shao, *Angew. Chem. Int. Ed.* **2009**, *48*, 8010 – 8013; *Angew. Chem.* **2009**, *121*, 8154 – 8157.

[18] S. Amemiya, Y. Wang, M. V. Mirkin in *Specialist Periodical Reports in Electrochemistry, Vol. 12*, (Eds.: R. G. Compton, J. D. Wadhawan), RSC Publishing, Cambridge, **2013**, pp. 1 – 43.

[19] a) P. K. Hansma, B. Drake, O. Marti, S. A. C. Gould, C. B. Prater, *Science* **1989**, *243*, 641 – 643; b) Y. E. Korchev, C. L. Bashford, M. Milovanovic, I. Vodyanoy, M. J. Lab, *Biophys. J.* **1997**, *73*, 653 – 658; c) C.-C. Chen, Y. Zhou, L. A. Baker, *Annu. Rev. Anal. Chem.* **2012**, *5*, 207 – 228.

[20] P. Elsamadisi, Y. Wang, J. Velmurugan, M. V. Mirkin, *Anal. Chem.* **2011**, *83*, 671 – 673.

[21] W.-J. Lan, D. A. Holden, B. Zhang, H. S. White, *Anal. Chem.* **2011**, *83*, 3840 – 3847.

[22] G. R. Willmott, B. E. T. Parry, *J. Appl. Phys.* **2011**, *109*, 094307.

[23] W.-J. Lan, H. S. White, *ACS Nano* **2012**, *6*, 1757 – 1765.

[24] a) H. Chang, F. Kosari, G. Andreadakis, M. A. Alam, G. Vasmatzis, R. Bashir, *Nano Lett.* **2004**, *4*, 1551 – 1556; b) R. M. M. Smeets, U. F. Keyser, D. Krapf, M.-Y. Wu, N. H. Dekker, C. Dekker, *Nano Lett.* **2006**, *6*, 89 – 95.

[25] W.-J. Lan, C. Kubeil, J.-W. Xiong, A. Bund, H. S. White, *J. Phys. Chem. C* **2014**, *118*, 2726 – 2734.

[26] M. A. Edwards, C. G. Williams, A. L. Whitworth, P. R. Unwin, *Anal. Chem.* **2009**, *81*, 4482 – 4492.

[27] R. Cornut, C. Lefrou, *J. Electroanal. Chem.* **2007**, *608*, 59 – 66.

[28] R. W. Clarke, A. Zhukov, O. Richards, N. Johnson, V. Ostanin, D. Klenerman, *J. Am. Chem. Soc.* **2013**, *135*, 322 – 329.

Received: September 24, 2014
Published online on December 8, 2014